

## The Use of Polarimetric Radar Data in Determining Lightning Cessation

Aaron D. Preston and Henry E. Fuelberg  
Florida State University, Tallahassee, FL

### 1. INTRODUCTION

#### 1.1 Research Motivation

The United States Air Force's 45<sup>th</sup> Weather Squadron (45WS) is responsible for providing weather forecast guidance to America's space program at Florida's Cape Canaveral Air Force Station (CCAFS), Kennedy Space Center (KSC), and Patrick Air Force Base (PAFB). This complex is located along the eastern coast of Florida's peninsula which is vulnerable to warm season thunderstorms. The greatest cloud-to-ground (CG) flash densities in the U.S. occur along the Florida peninsula during the warm season. This region, known as "lightning alley", receives 5 to 15 CG lightning strikes per square kilometer per year (Rudlosky, 2010). Lightning advisories are the most frequently issued weather advisory at CCAFS/KSC, making them a major concern for the daily operations of the complex since many ground-based activities must be suspended until the lightning threat has passed. Weather is responsible for 37% of launch delays and 47% of launch scrubs (McNamara, 2009).

Lightning is responsible for many deaths, injuries, and economic losses each year. Most people are not aware that there are more lightning-related fatalities each year in the U.S. than from either tornados or hurricanes. Forecasting lightning initiation and cessation is especially important because most lightning-related deaths occur before or after the most intense period of lightning activity when the threat is not as evident (Holle et al., 1992).

Forecasters at the 45WS are responsible for issuing and discontinuing lightning advisories for thirteen areas in the KSC/CCAFS region. Although the 45WS is reasonably satisfied with their ability to forecast lightning initiation, they need improved guidance to determine when it is safe to cancel an advisory (Roeder, personal

communication, 2012). The amount of time to wait until cessation truly has occurred remains problematic for operational forecasters, causing lightning advisories to remain in effect for too long. Improving lightning cessation forecasts will give forecasters confidence that a particular flash is the last of a given storm. This will enable lightning advisories to be terminated earlier and with more certainty than currently possible. This could save millions of dollars each year for launch operations, aviation industries, and other outdoor activities; but more importantly, it will save lives.

Recent advances in lightning and radar technology provide new perspectives on the occurrence of intra-cloud (IC) and CG flashes and their relation to storm-scale processes. Many recent studies suggest that dual-polarimetric radar can be used in conjunction with total lightning data to better understand the generation and dissipation of charge within thunderstorms (e.g., Bruning et al. 2007; Deierling et al. 2005; Deierling et al. 2008). The National Weather Service (NWS) currently is upgrading its WSR-88D radars to dual-polarimetric capability. Dual-polarimetric capability is essential for distinguishing between different types of hydrometeors and their vertical distribution. Our research examines the use of dual-polarimetric radar data to address the 45WS' need for improved guidance regarding lightning cessation at CCAFS/KSC. Our goal is to develop statistically and empirically derived lightning cessation algorithms using total lightning (CG and IC) and dual-polarimetric radar data that can be used operationally by the 45WS at CCAFS/KSC.

#### 1.2 Thunderstorm Electrification

Determining when the last flash has occurred within a particular storm cell is very difficult because of our lack of knowledge

regarding the processes that lead to thunderstorm electrification. The non-inductive charging (NIC) mechanism is the most well-known theory for how charge separation occurs in thunderstorms (Williams, 2001). Studies have shown that the transfer of charge within the updraft of the storm is due to collisions between ice crystals and graupel in the presence of supercooled water (e.g., Takahashi, 1978; Jayaratne et al. 1983; Saunders et al., 1991). Charge separation causes storms to develop a tripole charge structure, i.e., 1) a dominant negative charge region between  $-10^{\circ}\text{C}$  and  $-25^{\circ}\text{C}$ , 2) a positive region above the negative region, and 3) a weaker positive region below the negative region near  $0^{\circ}\text{C}$  as shown in Figure 1 (Krehbiel, 1986; Williams, 2001). IC flashes generally occur between the main negative and two positive charge regions (Shao and Krehbiel, 1995). Negative CG flashes originate from the dominant negative charge region (Krehbiel et al., 1979; Williams, 2001). Positive CG flashes can occur when thunderstorms contain a dominant positive charge region due to a reversal in polarity.

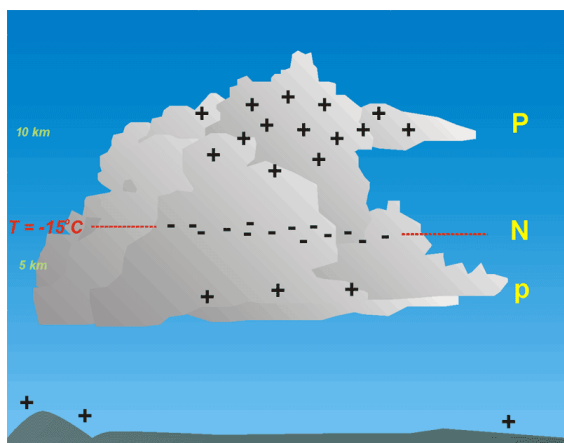


**Figure 1.** Typical tripole charge structure showing a dominant negative region between  $-10^{\circ}\text{C}$  and  $-25^{\circ}\text{C}$ , a positive region above this area, and a weaker positive region below this area near  $0^{\circ}\text{C}$ .

### 1.3 Previous Research

Several studies have examined lightning cessation based on studies of lightning initiation. Wolf (2006) showed that reversing the initiation criteria of 40 dBZ radar reflectivity above the  $-10^{\circ}\text{C}$  isotherm level held some promise for forecasting cessation. However, very few

studies specifically have examined lightning cessation. Hinson (1997) studied three storms in the KSC area using conventional radar. He found a lag time of  $\sim 30$  min between the last occurrence of 45 dBZ reflectivity at the  $-10^{\circ}\text{C}$  isotherm level and the last CG strike. Holmes (2000) expanded the dataset to 40 cases and noted that single and multi-cell storms required a different regression model to forecast cessation. Roeder and Glover (2005) found that 75% of the variation in times between the last and second-to-last CG flashes for storms near KSC could be fit to a log-linear curve. The findings of Roeder and Glover (2005) provided motivation for Stano et al. (2010, hereafter denoted ST10) to use total lightning data to develop empirical lightning cessation forecast guidance for KSC. ST10 used the Lightning Detection and Ranging (LDAR) network as the primary observational tool to investigate both CG and IC lightning. LDAR data and real-time sounding and radar parameters were used to create and analyze five statistical and empirical cessation schemes derived from 116 isolated thunderstorms near Cape Canaveral during the warm seasons of 2000-05. Correlations were identified between lightning cessation and parameters from the sounding and radar data. They found that the maximum interval, i.e., the greatest time between any two flashes of a storm, was the best parameter for investigating cessation. Their results provided motivation for the Melvin et al. (2010, denoted ME10), as well as for this study.

Prior research has shown that the vertical distribution of the various types of hydrometeors is related to the charging mechanisms needed for electrification. Dual-polarimetric radar data can distinguish between different types of hydrometeors, such as rain, hail, graupel, and categories of snow (Istok et al. 2009), as well as their vertical distribution.

### 1.4 Objectives

This study examines both radar and lightning characteristics during the period leading up to, and after, cessation. The lightning characteristics being examined include flash initiation heights and flash rates. Reflectivity, differential reflectivity, differential phase, specific differential phase, correlation coefficient, and hydrometeor classification at heights of different temperatures (i.e.,  $0^{\circ}\text{C}$ ,  $-10^{\circ}\text{C}$ ,  $-20^{\circ}\text{C}$ ) are analyzed to determine if inverting lightning

initiation criteria can help predict cessation. Changes in storm characteristics, such as heights of specific reflectivity values and vertical gradients of reflectivity also are analyzed during the minutes preceding cessation.

We believe that dual-polarimetric radar will provide new insights into lightning cessation. The following questions are addressed in this paper:

- i. Do dual-polarimetric radar data help in developing useful cessation algorithms?
- ii. What explains Melvin's lack of conclusive findings using conventional WSR-88D radar data?
- iii. What conditions occur prior to the last lightning flash?
- iv. Can these conditions be inferred from ground based sensors such as dual-polarized radar?

## 2. DATA AND METHODOLOGY

Our approach is similar to that of ME10; using the Warning Decision Support System – Integrated Information (WDSS-II) software (Lakshmanan et al., 2007). Storms were tracked using the WDSS-II K-means storm clustering and tracking algorithm. This algorithm identifies and tracks storm features (Lakshmanan et al. 2009) and extracts information from additional gridded fields (Lakshmanan and Smith 2009). This approach is ideal for time series analysis of radar, storm environment, and lightning characteristics.

### 2.1 Data Sources

Since the dual-polarimetric radar at Patrick Air Force Base (PAF) was delayed in becoming operational, we chose central Oklahoma as the domain of study.

#### 2.1.1 Lightning Data

The Oklahoma Lightning Mapping Array (OK-LMA) (Figure 2) measures the time and amplitude of the largest signal radiated by lightning during each 80-100  $\mu$ s period using a very high frequency (VHF) television band. OK-LMA detects sources from IC flashes and the upper portions of CG flashes, but due to the curvature of the earth, it cannot detect sources near the surface. Therefore, we merged OK-

LMA data with CG flash data to provide ground strike locations. This flash matching algorithm (McNamara, 2002) also was used by ST10 and ME10. Matches were based on temporal and spatial constraints. Each LMA initiation source had to be within 1 s and 5 km of the CG strike for it to be classified as the initiation point of a CG strike.

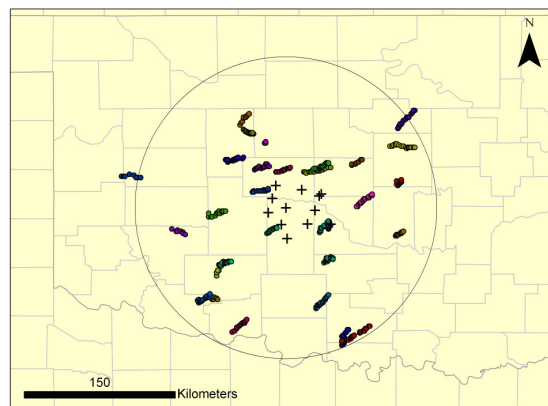


**Figure 2.** The research domain in central Oklahoma, where the radius is 150 km from the central OK-LMA receiver. Locations of the 11 sensors are shown (crosses), as well as the 30 storms we selected in central Oklahoma. The different colors represent the 30 different storm tracks at 1 min intervals.

The CG data in our study were collected using the National Lightning Detection Network (NLDN). The NLDN provides location, time, polarity, peak current, and multiplicity of CG flashes. Following the upgrade during 2002-03, it has a 90-95% detection efficiency (DE) and ~500 m location accuracy (Cummins and Murphy 2009; Cummins et al. 2006)

#### 2.1.2 Dual-Polarimetric Radar Data

Dual-polarimetric radar data were obtained from the KOUN S-Band radar to locate storms, determine which flashes coincided with each storm, create radar-derived products, and derive storm characteristics. The archived Level-II reflectivity data were obtained from the National Climatic Data Center [<http://has.ncdc.noaa.gov>]. Dual-polarimetric radar provides three new base products that are not available from conventional WSR-88D radars. These include differential phase, correlation coefficient, and differential reflectivity.

Differential phase (PhiDP) is the difference in phase between the horizontal and vertical returned energy. Specific differential phase (Kdp) is the range derivative of PhiDP as given by equation (1). It is used to determine where along the propagation path the phase changes are occurring. Kdp typically ranges from  $-1^{\circ} \text{ km}^{-1}$  to  $6^{\circ} \text{ km}^{-1}$  for meteorological echoes. Positive Kdp indicates that the horizontal pulse has increased more rapidly than the vertical pulse. This occurs when there is more scattering from hydrometeors oriented in the horizontal plane than the vertical plane (i.e., oblate hydrometeors). Negative Kdp indicates vertically oriented hydrometeors, and Kdp near zero indicates spherical hydrometeors (i.e., hail). Kdp is very helpful in estimating rainfall.

$$Kdp = \frac{PhiDP(r2) - PhiDP(r1)}{2(r2 - r1)} \text{ [}^{\circ} \text{ km}^{-1}\text{]} \quad (1)$$

where,

$$PhiDP = \Phi_h - \Phi_v \text{ [}^{\circ}\text{]}$$

$$\Phi_h \geq 0, \quad \Phi_v \geq 0$$

Our question is whether Kdp can help infer when lightning activity has ceased? Kdp has been shown to decrease prior to a flash as ice crystals become vertically aligned due to an increasing electric field. Once a flash occurs, the ice crystals and electric field “relax”, which is indicated by an increase in Kdp. The top panel of Figure 3 shows a storm before a lightning flash, while the bottom panel shows the storm at the approximate time of the flash. Kdp exhibits an abrupt increase, or relaxation, after the flash occurs. We hypothesize that this strong vertical alignment “signature” of the electric field in Kdp will disappear as the storm nears cessation.

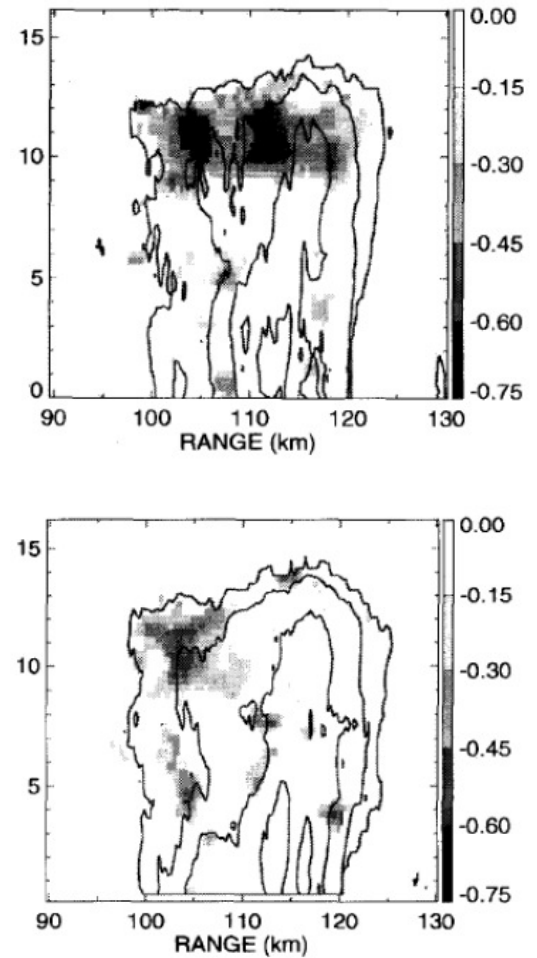


**Figure 3.** Cross section of specific differential phase (Kdp) through a storm before (top) and during (bottom) a lightning flash. The large area of negative Kdp disappears, and becomes more positive, seconds after the flash occurs. (After Anderson 2008; Caylor and Chandrasekar 1996)

Correlation coefficient (RhoHV) is another base product of dual-polarimetric radar. It measures the correlation between horizontal and vertical back scattered power. RhoHV mainly is used to determine the uniformity of hydrometeors. We did not find any utility in using RhoHV to indicate cessation, and therefore it will not be discussed further.

Differential reflectivity (Zdr) compares the relative horizontal and vertical orientations of hydrometeors. This can help identify the presence of supercooled water ( $Zdr > 1$  dB above the melting layer) and the melting layer ring ( $Zdr$  between 0.5 and 2.5 dB).  $Zdr$  exceeding 2 dB is associated with rain,  $Zdr$  near

zero is associated with hail, and negative Zdr indicates graupel.

We also used the upgraded WDSS-II hydrometeor classification algorithm (HCA) as described in Scharfenberg (2006). The HCA identifies different hydrometeor types and assigns a particle identification (PID) value to each particle. This allows us to identify regions of high graupel and hail concentrations within the mixed phase region of a storm's core.

The vertical distribution of the various types of hydrometeors is related to the charging mechanisms needed for electrification. Several recent studies suggest that dual-polarimetric radar, used along with total lightning data, can provide insight into the generation and dissipation of charge within individual storms (Bruning et al. 2007; Deierling et al. 2005; and Deierling et al. 2008).

Bruning et al. found observational evidence that local maxima in graupel concentrations are well correlated in space and time with the initiation locations of lightning flashes. The correlation between lightning initiation and higher graupel concentrations suggests that graupel can enhance the electric field past the threshold for lightning initiation. Deierling et al. (2005) found that the relationship between hail mass and total lightning is not as strong as between graupel mass and total lightning. This suggests that graupel plays a more dominant role in thunderstorm electrification than hail. We hope to verify the correlation between graupel concentration and lightning production by examining the WDSS-II PID algorithm as cessation nears. We also wish to determine whether flash initiation sources (i.e., the first source to be detected within an individual flash) are closely located with regions of graupel.

### 2.1.3 Rapid Update Cycle Data

We used archived National Centers for Environmental Prediction (NCEP) Rapid Update Cycle (RUC) model analyses (Benjamin et al. 1994; 2004) to describe storm environments in central Oklahoma for use in WDSS-II. Hourly RUC analyses were available at 20 km grid resolution between 2010-11. These data were obtained from the Atmospheric Radiation Measurement (ARM) Program. The RUC data are critical to obtain the heights of the 0°C, -10°C, and -20°C environmental temperatures.

The KOUN radar data and RUC model analyses were merged using the WDSS-II software. This merging does not wait until a volume scan is completed. Instead, the volume scan is updated as data from each elevation scan become available, thus allowing merged reflectivity, differential reflectivity, differential phase, specific differential phase, correlation coefficient, and particle identification products to be output every minute.

## 2.2 Methodology

### 2.2.1 Research Domain and Time Period

Our research domain had a radius of 150 km from the central receiver of the OK-LMA (Figure 4, ring). This domain includes the 11 lightning sensors within the radar coverage of KOUN.

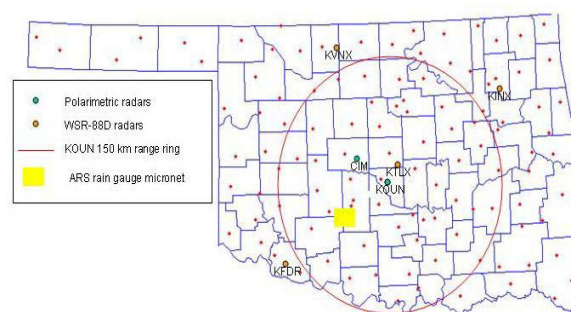


**Figure 4.** We used the KOUN S-Band dual-polarimetric radar data out to a range of 150 km. (After Ryzhkov and Giangrande 2004)

Synoptic forcing is weak during Florida's warm season, and most thunderstorms are initiated by local heating and sea breeze convergence. This produces scattered, isolated thunderstorms that are challenging to forecast. We strived to find similar "pulse-like" storms in central Oklahoma. We sought isolated storms since they are the easiest to assign individual flashes.

### 2.2.2 Ingesting Lightning Data

We used the flash consolidation algorithm within WDSS-II to combine individual OK-LMA sources into flashes (Lakshmanan et al., 2007). This algorithm groups VHF sources that occur within a specified time and distance of each other into a single flash event. We used a time threshold of 300 ms, with the distance threshold (km) being proportional to the distance that the source is detected from the center of the LMA

network. Although the default time threshold inherent to WDSS-II is 250 ms, we used the more lenient time threshold of 300 ms based on previous research (Scott Rudlosky, personal communication, 2010). Furthermore, at least three collocated, simultaneous VHF sources were required to define a flash (Scott Rudlosky, personal communication, 2010). This allowed us to ignore singletons (i.e., one source point) and small flashes containing only two sources. These flashes comprised ~ 52% of the total flashes detected within range of the OK-LMA; however, many of them were noise, not lightning. Only flashes consisting of three or more source points were used to calculate total flash rates.

Finally, we used the default distance threshold inherent to the flash creation algorithm. Specifically, equation (2) determined the distance threshold for consolidating sources into a single flash event:

$$D1 (1 + D2 (r - D3)^2), \text{ where } (2)$$

$$D1 = 5, D2 = 0.00001, D3 = 100, \text{ and } r = \text{range from OK-LMA network center}$$

This consolidation procedure allowed us to reconstruct IC channels and the upper portions of CG flashes. The IC channels then could be viewed within the WDSS-II graphical user interface (GUI) and overlaid with CG flash locations, radar, and model-derived data.

Although the NLDN operates in the low-frequency (LF) and very low-frequency (VLF) bands, it detects some IC flashes and in-cloud components of CG flashes (Cummins and Murphy 2009). Cummins et al. (1998) recommended that +CG reports with a peak current  $I_p < 10$  kA be considered IC flashes unless confirmed otherwise. Later, Biagi et al. (2007) determined that +CG strikes with  $I_p < 15$  kA were more likely cloud pulses than actual CG flashes. Based on these recent results, we used the 15 kA threshold to separate weak CG from IC flashes.

### 2.2.3 K-Means storm clustering and tracking algorithm

The K-Means storm clustering and tracking algorithm was very important to the success of this study. The algorithm identifies and tracks features contained in lightning and radar data

(Lakshmanan et al. 2009) and extracts information about them and from environmental parameters, such as from RUC (Lakshmanan and Smith 2009). Fields of the specified parameters were tracked if they exhibited a minimum cell size of 10-15 km<sup>2</sup>, depending on the parameter used for tracking. We used Vertically Integrated Liquid (VIL) Density and merged reflectivity composite products to track individual cells. VIL is a derived product of vertically integrated reflectivity, representing the equivalent liquid water content based on drop-size distributions. VIL Density is merely VIL divided by the echo top. It is often used to identify storms with large reflectivities relative to their heights. Large values of VIL Density can indicate a deeper, more intense hail core, and can be used as a proxy for hail size (Amburn and Wolf, 1996). The clusters tracked using VIL Density and merged reflectivity composites were compared to determine which produced the best track. Thus, for some storms, both tracking products were used during a storm's lifetime. However, since values of VIL Density are small or nonexistent in a storm's anvil, clusters tracked using this product did not capture the anvil region. This became problematic for some cases in which lightning occurred within the anvil region. These storms were tracked, almost exclusively, using only the merged reflectivity composite.

The tracking procedure was automated, producing a database at 1 min intervals that described the lightning and radar characteristics of the storm. Gridded information then could be extracted from these tracked clusters (e.g., average, minimum, or maximum values) to create time series plots. One should note that the WDSS-II K-Means storm clustering and tracking algorithm is far from perfect. It is primarily used to track storms near peak intensity when they present a threat to the public. Our tracking of weakening storms through cessation was no trivial task. To ensure the best tracking possible, a running smoothing operator was implemented to dilate the merged reflectivity composites. This expanded the areas of reflectivity in an 11 × 11 gridded neighborhood, expanding the maximum areas of reflectivity and allowing storms to be tracked for longer periods. However, even with this smoothing, the tracking algorithm often was unable to consistently track a cell throughout its lifetime. Since the clusters tended to contract in size as the storm dissipated, maximum and

minimum values of the WDSS-II output parameters were favored over average values which relied too heavily on the size of the cluster being tracked. All storms that were selected were visually examined to ensure that they met the specified criteria and were tracked consistently.

### 2.2.4 Selecting Storms

Pulse thunderstorms in Oklahoma were chosen to represent the types of warm season thunderstorms commonly observed at KSC/CCAFS. We currently have examined 30 storms (Figure 2) spanning three different days (Table 1) during the warm-seasons of 2010-11 that were within 150 km of the center of the OK-LMA network. Since the National Weather Service radar in Melbourne, Florida (KMLB) was recently upgraded to dual-polarimetric capability, future additional study days will be selected from the 2012 warm season in both central Oklahoma and the KSC/CCAFS region to build a more robust dataset. Only the eight storms (Table 1, bold) occurring on 14 May 2010 were used to compute statistics and plots that follow.

**Table 1.** Distribution of the 30 storms in our dataset. These storms occurred on three different days during 2010 -11. The left column indicates the date (year, month, day), and the right column is the total number of storm cells selected from that date that have been examined.

<b>Case date</b>	<b>Storm Cells</b>
<b>20100514</b>	<b>8</b>
20110611	10
20110712-13	12

We compared the environmental conditions, duration, and maximum reflectivity of the 30 storms in central Oklahoma to 20 typical warm season storms in the KSC/CCAFS region (Table 2). Results suggest that the Oklahoma storms are a reasonable surrogate to those in central Florida.

**Table 2.** Comparison of average values from 20 storms in KSC/CCAFS and 30 storms in central Oklahoma.

	KSC/CCAFS	Central Oklahoma
BRN Shear	6.2 m/s	13.5 m/s
MUCAPE	1700 J/kg	1400 J/kg
Maximum Reflectivity	54 dBZ	52.5 dBZ
Duration	49 min	78 min

Storms were only included in the final dataset if they fell into all five of the following categories:

- 1) Contain lightning activity,
- 2) Isolated single-cell pulse storm, i.e., not multicellular or linear,
- 3) Exhibits similar features to KSC storms, i.e., not supercellular or too severe,
- 4) Storm within 150 km radius study domain, and
- 5) Storm tracked through cessation, i.e., no discontinuity in storm tracking using the K-Means storm clustering and tracking algorithm

Thousands of storms were removed from our final dataset for not meeting the last criterion. They could be tracked properly during the middle of their lightning activity, but the tracking stopped several minutes before cessation occurred as the storm weakened.

We selected three days based on the quantity and type of trackable storms on those days. We sought days that had 10 + storms that were tracked well by WDSS-II. We also made sure that these storms had pulse-like behaviors similar to those that form near KSC/CCAFS. We did not wish to examine supercellular storms. Values of Convective Available Potential Energy (CAPE) and Bulk Richardson Number (BRN) on the selected days are similar to those that occur near the KSC/CCAFS region (Table 2). The convection in Oklahoma on these days was initiated along a stationary front in advance of an upper-level trough, in a manner similar to KSC/CCAFS storms that develop along sea breeze frontal boundaries. We did not consider days when convection was initiated by a dry line.

### 3. PRELIMINARY RESULTS

#### 3.1 Time-Trends in Lightning Characteristics of 8 Storms.

**Table 3.** Flash characteristics of the 8 storms examined on 14 May 2010. Data from the remaining 22 storms currently are being studied.

Entire Storm Duration	30 min to 80 min
Period Tracked Before Cessation	11.4 min 29.4 min
Flash Rate	2 to 6 min <sup>-1</sup>
Median Flash Rate	2.5 min <sup>-1</sup>
Source Rate	13 to 182 min <sup>-1</sup>
Median Source Rate	78 min <sup>-1</sup>
IC Flashes	94
CG Flashes	25
% storms with CG flashes	6 of 8 (75%)
Type of last flash	100% IC / 0% CG
IC:CG ratio	79.0% IC / 21.0% CG
% Positive CG	2 (8.0%)
% Negative	23 (92.0%)
Average IC Initiation Altitude	7.5 km
Average CG Initiation Altitude	5.8 km

The lightning characteristics shown in Table 3 are based on only 8 of our 30 storm dataset. The remaining 22 storms are still being examined. The 8 storms produced 119 total lightning flashes, including 25 CG strikes during the period each storm was tracked prior to cessation (~ 15 min). None of the storms was associated with any storm reports. It is interesting to note that none of the 8 storms produced a CG flash as the final flash. The flash rates (min<sup>-1</sup>) and source rates (min<sup>-1</sup>) are defined as the maximum observed rates during the period each of the 8 storms was tracked. The source rates are much more variable than the flash rates. The mean IC and CG initiation heights are consistent with values from previous studies (ME10). The CG flashes generally initiate at lower altitudes than IC flashes (Table 3). The IC flashes originate at an average altitude of 7.5 km, while the CG flashes originate at an average altitude of 5.8 km. The average maximum heights of the 0°C, -10°C, and -20°C temperature levels for the subset of 8 storms is 4.1 km, 5.4 km, and 7.1 km, respectively. This indicates that IC flashes tend to originate near the -20°C temperature level, whereas CG flashes originate at lower levels (near -10°C).

This is consistent with previous studies and the tripole charge structure (Figure 1).

#### 3.2 Case Study Example

Single Cell on 14 May 2010

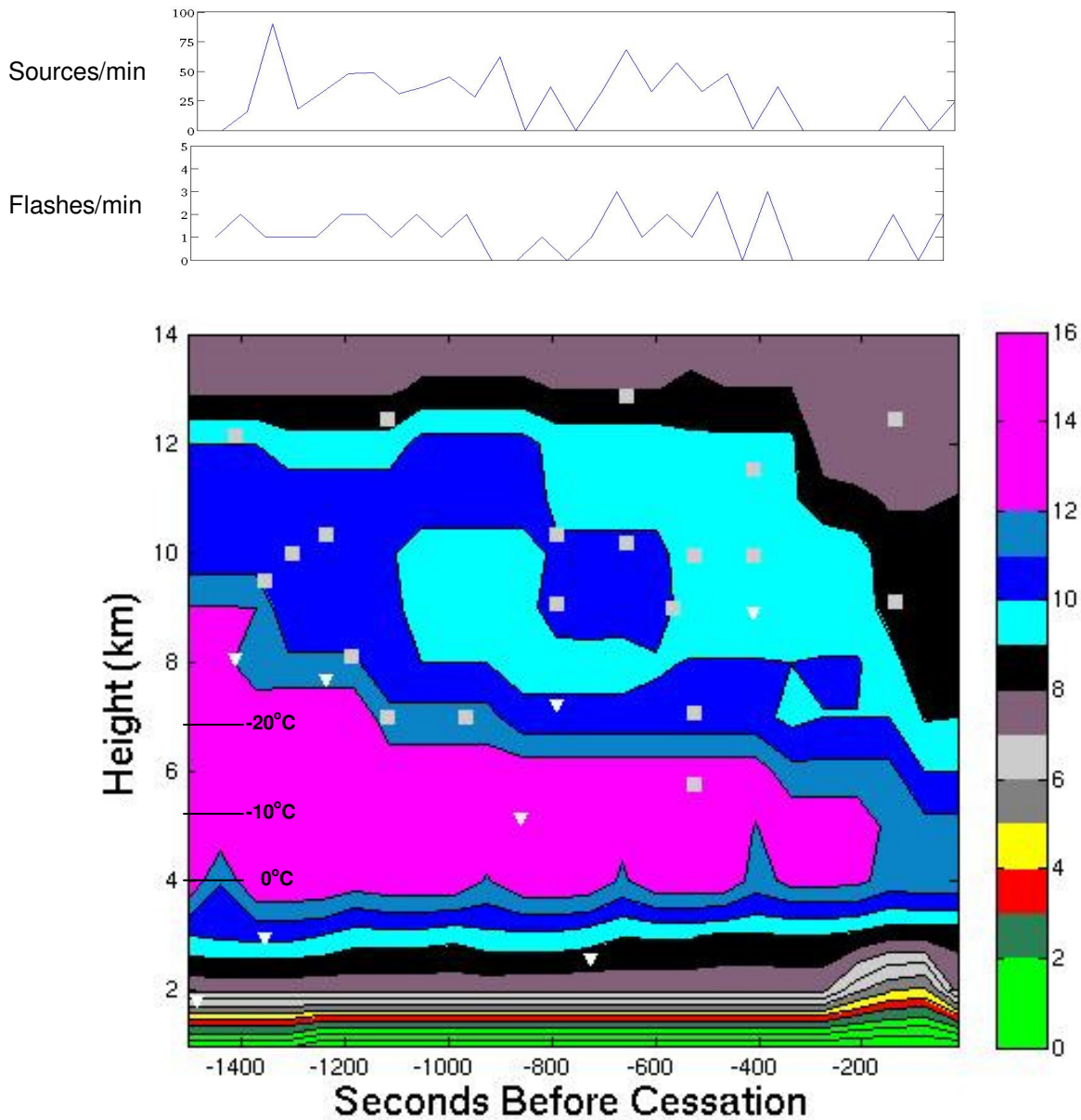
Time-height plots of several radar parameters were created to gain insight on storm characteristics and hydrometeor distributions as a storm nears cessation. Figure 5 is the time-height plot of PID, showing the vertical distribution of hydrometeors with LMA initiation sources overlaid. The WDSS-II derived PID categories for the plot in Figure 5 are listed in Table 4. IC flashes originate anywhere from 6 to 12 km, between the main negative and upper positive charge regions. Most of the CG flashes originate between 2 and 8 km in close proximity to the main negative charge region. This is consistent with previous studies (Shao and Krehbiel, 1995). Figure 6 is the time-height plot of conventional reflectivity. The 40 dBZ echo descends below the height of -10°C by the time of the last lightning flash, an IC flash at 0608:29 UTC. Figure 7 is the time-height plot of specific differential phase. A positive phase shift, indicating hydrometeors becoming more horizontally oriented, occurs during the 1200 to 400 s (~ 20 to 6 min) period before the last lightning flash,  $t = 0$ .

#### 3.3 Storm Characteristics during the Minutes Leading to Lightning Cessation

Our results expand on those of ME10 who examined conventional reflectivity at 0°C, -10°C, and -20°C. ME10 found no convergence of reflectivity to a specific value at any altitude as cessation neared. Nonetheless, they determined that the -10°C temperature level had the greatest potential for indicating that lightning activity had ceased. This is expected since the most critical component of electrification (i.e., graupel concentrations in the main negative charge region) occurs in the -10°C to -15°C temperature layer. Therefore, although we looked at dual-polarimetric products at various temperature levels (e.g., 0°C, -10°C, -20°C), we were especially interested in what was happening at the -10°C temperature altitude before and after cessation. We currently are developing cessation algorithms, and hypothesize that the best cessation algorithm will involve thresholds from more than one dual-polarimetric product.







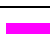


## Vertical PID Profile for Single Cell on 14 May 2010



**Figure 5.** Time-series of the vertical distribution of hydrometeors of cluster-derived maximum PID values (color shaded) obtained from the WDSS-II HCA algorithm. IC and CG flash initiation sources (squares and triangles, respectively) are overlaid for a single cell storm on 14 May 2010. The resolution of the cluster-derived PID values is 1 km at ~ 1 min time resolution. Flash initiation heights were obtained from raw OK-LMA data. Source and flash rates during the same time period are shown in the top two panels, respectively. Cluster-derived maximum heights of the environmental 0°C, -10°C, and -20°C isotherm levels can be seen on the left hand side of the figure. These values were obtained from RUC hourly analyses.

**Table 4.** The WDSS-II PID classification contains 12 bulk hydrometeor categories. The following shows only the categories significant to this research.

Value	Color	WDSS-II PID
0-2		Light/Moderate Rain
2-3		Heavy Rain
3-4		Rain/Hail
9-10		Dry Snow
10-11		Wet Snow
11-12		Ice Crystals
12-14		Graupel

## Vertical Reflectivity Profile for Single Cell on 14 May 2010

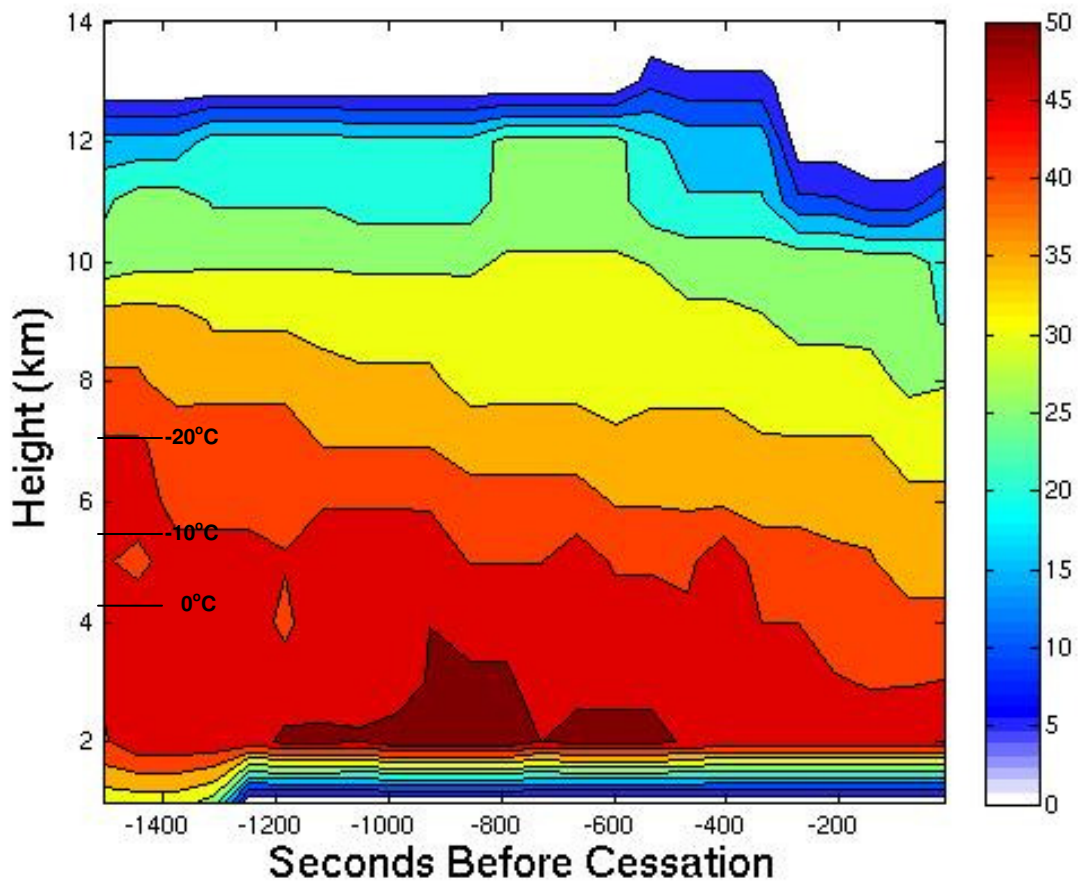


**Figure 6.** As in Figure 5 (same single cell), except showing maximum conventional reflectivity (color shaded, dBZ).

## Vertical Specific Differential Phase Profile for Single Cell on 14 May 2010

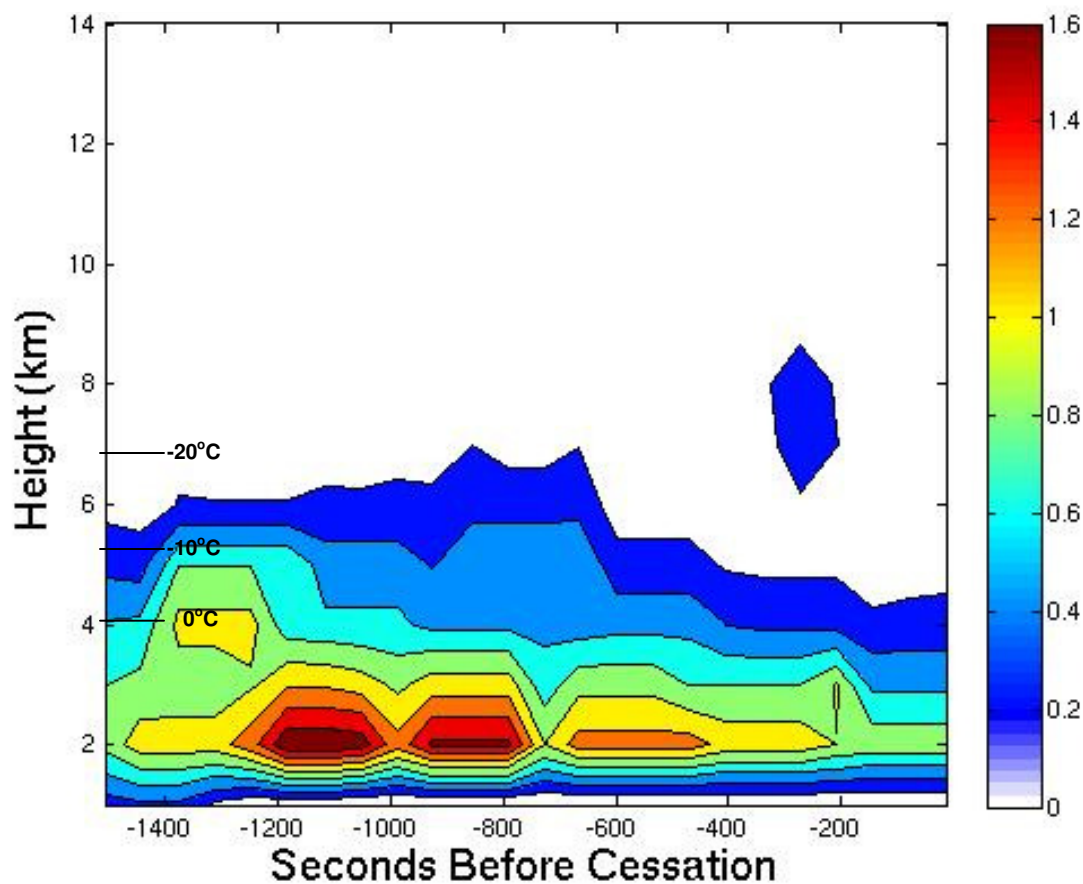
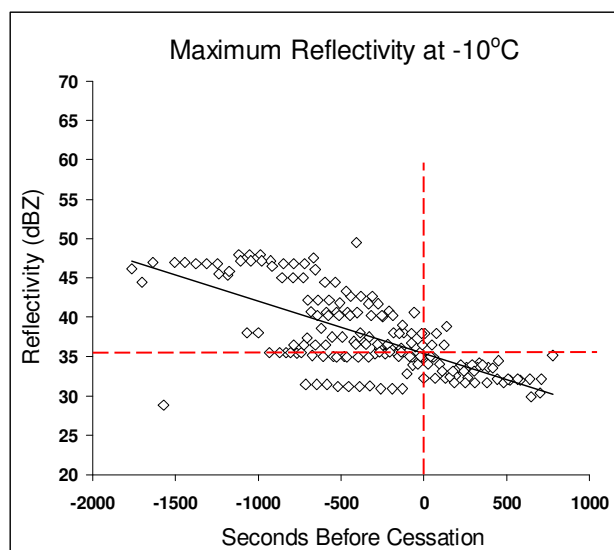


Figure 7. As in Figure 5 (same single cell), except showing maximum specific differential phase (color shaded, degrees).

### 3.3.1 Radar Reflectivity at Different Temperature Levels

We examined conventional reflectivity ( $Z_h$ ) at different temperature levels, including maximum reflectivity at the environmental  $0^\circ\text{C}$ ,  $-10^\circ\text{C}$ , and  $-20^\circ\text{C}$  levels within each storm cluster. The maximum reflectivity at  $-10^\circ\text{C}$  is plotted at 1 min intervals in Figure 8. This

parameter decreased more (5 dBZ) than reflectivity at any other altitude during the 10 min period prior to cessation, from 40.5 dBZ to 35.5 dBZ. The values seem to converge to  $\sim 35$  dBZ at the time of cessation (red-dashed line). We believe this parameter might be useful to predict cessation, but not on its own. We hope to use it in combination with various dual-polarimetric parameters in a multiple threshold cessation algorithm.



**Figure 8.** Time trend of maximum reflectivity (Zh, dBZ) at  $-10^{\circ}\text{C}$  at 1 min intervals. The 35 dBZ echo descends below  $-10^{\circ}\text{C}$  in almost all of the storms by the time of the last flash,  $t = 0$ .

### 3.3.2 Specific Differential Phase at Different Temperature Levels

The previously described studies noted a decrease in Kdp prior to a flash as the electric field became more vertically aligned (Anderson, 2012). Therefore, we expect a prolonged relaxation of the electric field, or increasing Kdp, after the last lightning flash. Each of the 8 storms examined in Figure 9 show spikes (circled in red) in maximum Kdp (above  $0.2^{\circ}$ ) at the  $-10^{\circ}\text{C}$  temperature level, indicating hydrometeors becoming more horizontally oriented. However, the overall pattern does not show a convergence or plateau of values as we expected. The convergence of minimum Kdp values toward  $-0.1^{\circ}$  at  $-10^{\circ}\text{C}$  (Figure 10) shows more promise than maximum Kdp values in determining when lightning activity has ceased. All 8 storms have minimum cluster-derived Kdp values above  $-0.19^{\circ}$  (red-dashed line) after the last lightning flash,  $t = 0$ . Some of these storms had minimum Kdp values below  $-0.19^{\circ}$  prior to cessation. This indicates a weakening in the vertical alignment of the electric field at the time of cessation.

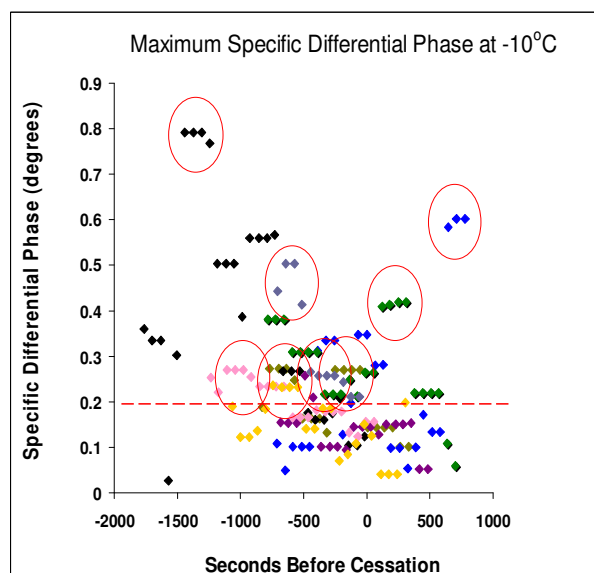


**Figure 9.** Time trend of maximum specific differential phase (degrees) at  $-10^{\circ}\text{C}$  at 1 min intervals. The different colors represent the 8 different storms examined. Substantial spikes (circled in red), indicating positive phase shifts, occur at various time before and after the last flash at,  $t = 0$ .

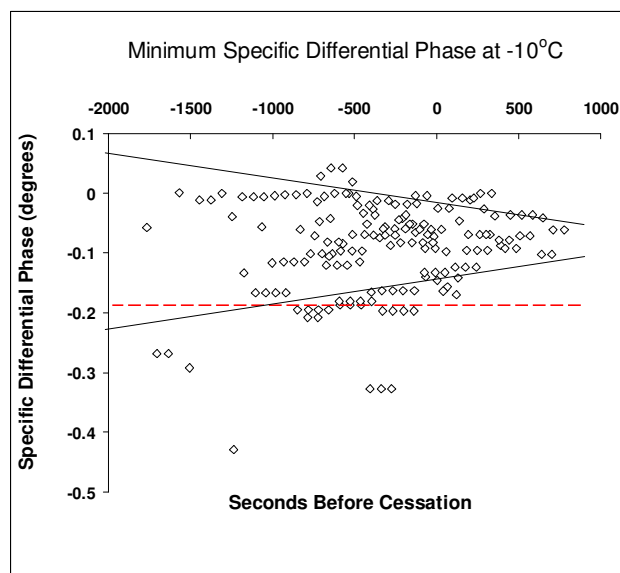


**Figure 10.** As in Figure 9, except for minimum specific differential phase at  $-10^{\circ}\text{C}$ .

### 3.3.3 Differential Reflectivity at Different Temperature Levels

Figures 11a and 11b indicate no relationship between differential reflectivity and time to cessation. Woodard et al. (2012) considered the first occurrence of

- (1)  $Z_{dr} > 0.5$  dB and  $Z_h > 35$  dBZ
- (2)  $Z_{dr} > 0.5$  dB and  $Z_h > 40$  dBZ
- (3)  $Z_{dr} > 1.0$  dB and  $Z_h > 35$  dBZ
- (4)  $Z_{dr} > 1.0$  dB and  $Z_h > 40$  dBZ

at  $-10^{\circ}\text{C}$ ,  $-15^{\circ}\text{C}$ , and  $-20^{\circ}\text{C}$  to develop an algorithm to forecast the first lightning flash within a storm. We tried inverting these thresholds to see if they exhibited utility for forecasting cessation. However, we found no utility based on poor statistical results.

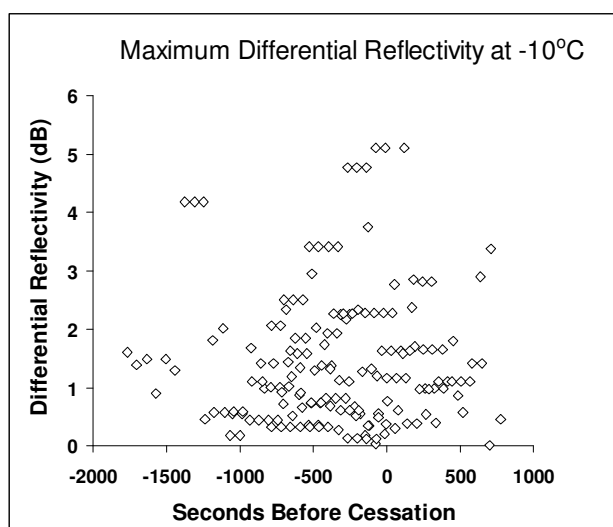


**Figure 11a.** Time trend of maximum differential reflectivity (dB) at  $-10^{\circ}\text{C}$  at 1 min intervals.

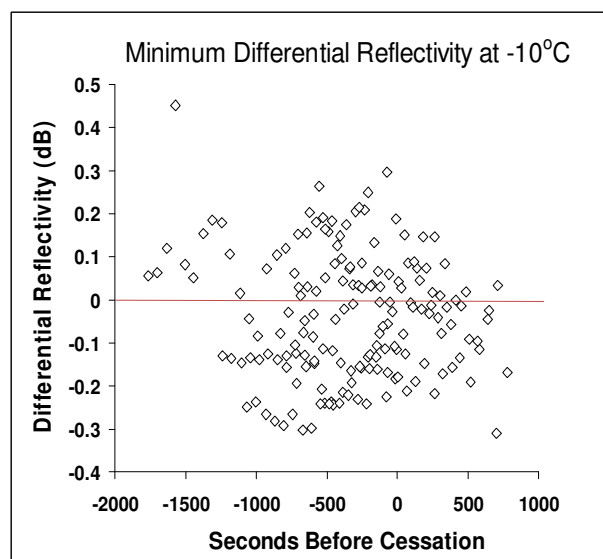


**Figure 11b.** As in Figure 11a, except for minimum differential reflectivity at  $-10^{\circ}\text{C}$ .

### 3.3.4 PID Classification at Different Temperature Levels

Maximum PID values at 1 min intervals are plotted at both  $0^{\circ}\text{C}$  (Figure 12) and  $-10^{\circ}\text{C}$  (Figure 13). Regions with high graupel concentrations (PID values of 12-14) disappear at both temperature levels at the time of cessation. This corroborates the findings of Bruning et al. by showing a strong relationship between lightning activity and graupel concentration. PID generally seems to exhibit more utility in indicating cessation than any other dual-polarimetric parameter examined.

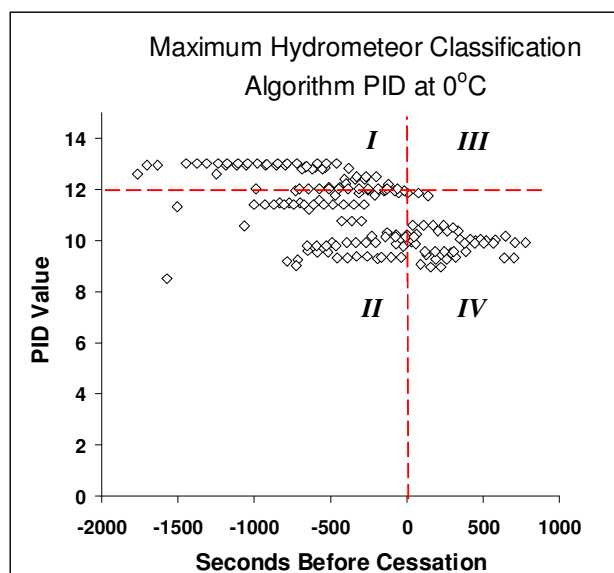


**Figure 12.** Time trend of the WDS-II PID classification at  $0^{\circ}\text{C}$  at 1 min intervals. It is important to note the absence of any PID values exceeding 12 after the last lightning flash,  $t = 0$  (Quadrant III). This indicates no regions of graupel within the storm's core at the freezing level after lightning activity has ceased.

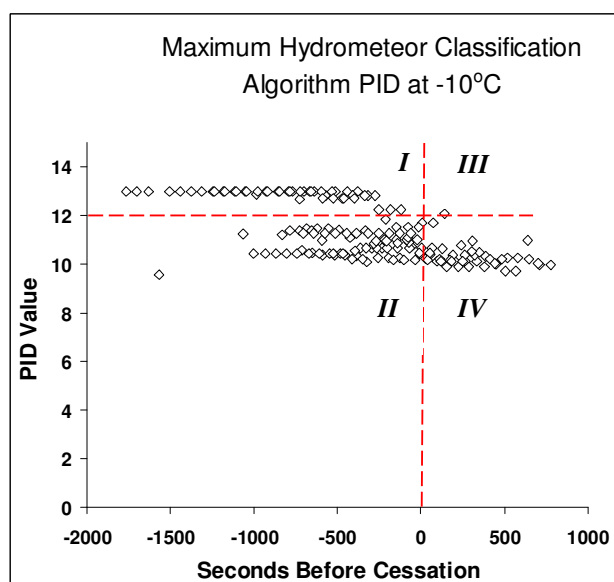


**Figure 13.** As in Figure 12, except for PID classification at  $-10^{\circ}\text{C}$ . As in Figure 12, there are no PID values in Quadrant III after the last lightning flash. This indicates no regions of graupel near the bottom of the main negative charge region of the storm's core ( $-10^{\circ}\text{C}$ ).

#### 4. SUMMARY AND CONCLUSIONS

We have examined trends in reflectivity, differential reflectivity, specific differential phase, and PID classification at three temperatures (i.e.,  $0^{\circ}\text{C}$ ,  $-10^{\circ}\text{C}$ ,  $-20^{\circ}\text{C}$ ) for 8 storms in central Oklahoma. Results show potential for determining cessation using reflectivity, specific differential phase, and PID classification. Differential reflectivity is the least reliable parameter for predicting cessation. We found no relationship between differential reflectivity and time to cessation (Figures 11a and 11b). We also found no utility in inverting the Zdr and Zh thresholds examined by Woodard et al. to forecast lightning cessation.

Storm characteristics of the 8 cells tracked by WDS-II were studied. We currently are examining the remaining 22 storms in our dataset. So far, our results indicate that the  $-10^{\circ}\text{C}$  temperature level holds the greatest promise for indicating cessation. Dual-polarimetric products at this temperature level increased or decreased most drastically near cessation or showed signs of convergence at the time of the last lightning flash.

Our study is motivated by the 45WS' need to improve lightning cessation guidance. While there have been many studies addressing lightning initiation, few have specifically examined lightning cessation. So far only 8 storms of our 30 storm dataset have been examined for storm and lightning trends prior to cessation. Our initial results are promising, indicating that a multiple threshold cessation algorithm using some combination of reflectivity, specific differential phase, and/or PID values may be successful in safely ending lightning advisories in a timely manner. In order to increase confidence in our results, we will continue to add more storms to our dataset from central Oklahoma (KOUN) and the KSC/CCAFS region (KMLB).

#### 5. FUTURE WORK

We are developing cessation algorithms based on the sample of 30 storms from central Oklahoma. We then will choose an independent dataset of storms ( $\sim 10$ ) from the KSC/CCAFS region, using the newly implemented dual-polarimetric radar in Melbourne (KMLB). These storms will be used to test how well each

cessation algorithm performs. Various skill statistics, such as probability of detection (POD), false alarm rate (FAR), critical success index (CSI), true skill statistic (TSS), and Heidke Skill Score (HSS) will be computed to determine which algorithm performs best.

## 6. ACKNOWLEDGEMENTS

We would like to thank Bill on IV on MacGorman for providing the OK-LMA lightning data. Additional support was provided by the Tallahassee National Weather Service Forecast office for providing the NLDN data. We would like to thank fellow Florida State alumni Geoffrey Stano, Holly Melvin, and Scott Rudlosky for providing valuable insight and guidance with this research. We would also like to thank Valliappa Lakshmanan and Jeff Brogden for their WDSS-II support. This research was funded by the U.S. Air Force under Contract FA2521-11-P-0091. Finally, we appreciate the continued interest and support provided by Mr. Bill Roeder of the 45<sup>th</sup> Weather Squadron

## 7. REFERENCES

- Amburn, S. and P. Wolf, 1996: VIL density as a hail indicator. Preprints, *18<sup>th</sup> Conf. Severe Local Storms*. Amer. Meteor. Soc., San Francisco, CA.
- Anderson, A., 2008: Inferring storm electrification through specific differential phase shift changes, AT 741 Final Project. Colorado State University. Available at [http://radarmet.atmos.colostate.edu/~aanderson/courses/radar\\_final.pdf](http://radarmet.atmos.colostate.edu/~aanderson/courses/radar_final.pdf)
- Benjamin S. G., K. J. Brundage, P. A. Miller, T. L. Smith, G. A. Grell, D. Kim, J. M. Brown, and T. W. Schlatter (1994), The Rapid Update Cycle at NMC. Preprints, *10<sup>th</sup> Conf. on Numerical Weather Prediction*, Portland, OR, Amer. Meteor. Soc., 566-568.
- \_\_\_\_\_, D. Devenyi, S. S. Weygandt, K. J. Brundage, J. M. Brown, G. A. Grell, D. Kim, B. E. Schwartz, T. G. Smirnova, T. L. Smith, and G. S. Manikin (2004), An Hourly Assimilation-Forecast Cycle: The RUC. *Mon. Wea. Rev.*, **132**, 495-518.
- Biagi, C. J., K. L. Cummins, K. E. Kehoe, and E.P. Krider, 2007: National Lightning Detection Network (NLDN) performance in southern Arizona, Texas, and Oklahoma in 003-2004, *J. Geophys. Res.*, **112**, D05208, doi:10.1029/2006JD007341.
- Bruning, Eric C., W.D. Rust, T. J. Schuur, D. R. MacGorman, P. R. Krehbiel, and W. Rison, 2007: Electrical and polarimetric radar observations of a multicell storm in TEXAS. *Mon. Wea. Rev.*, **135**, 2525-2544.
- Caylor, I.J., and V. Chandrasekar, 1996: Time-Varying ice crystal orientation in thunderstorms observed with multiparameter radar. *IEEE Trans. Geosci. Remote Sensing*, **34**, 847-858
- Cummins, K. L., M.J. Murphy, E. A. Bardo, W. L. Hiscox, R. B. Pyle, and A. E. Pifer, 1998: A combined TOA/MDF technology upgrade of the U.S. National Lightning Detection Network, *J. Geophys. Res.*, **103**, 9035-9044.
- \_\_\_\_\_, J.A. Cramer, C.J. Biagi, E.P. Krider, J. Jerauld, M.A. Uman, and V.A. Rakov, 2006: The U.S. National Lightning Detection Network: Postupgrade status. Preprints, 2<sup>nd</sup> Conference on Meteorological Applications of Lightning Data, January 29-February 2, Atlanta, GA, American Meteorological Society, 9 pp.
- \_\_\_\_\_, Murphy M., 2009: An overview of lightning locating systems: History, techniques, and data uses, with an in-depth look at the U.S. NLDN, *IEEE Trans. on Electromagnetic Compatibility*, 51 (3), 499-518.
- Deierling, W., J. Latham, W. A. Petersen, S. Ellis, H. Christian, 2005: On the relationship of thunderstorm ice hydrometeor characteristics and total lightning measurements. *Atmos. Res.*, **76**, 114-126.
- \_\_\_\_\_, W. A. Petersen, L. Latham, S. E. Ellis, and H. J. Christian, Jr., 2008: The relationship between lightning activity and ice fluxes in thunderstorms. *J. Geophys. Res.*, **113**, D15210, doi:10.1029/2007JD009700.

- Hinson, M. S., 1997: A study of the characteristics of thunderstorm cessation at the NASA Kennedy Space Center, M. S. Thesis, Aug 97, Texas A&M University, 91 pp.
- Holle, R. L., A. I. Watson, R. E. Lopez, K. W. Howard, R. Ortiz, and L. Li, 1992: Meteorological studies to improve short range forecasting of lightning/thunderstorms within the Kennedy Space Center area. Final Report, National Severe Storms Laboratory, NOAA, Boulder, CO, 91 pp. [Available from R. Holle, National Severe Storms Laboratory, 1313 Halley Circle, Norman, OK 73069.
- Holmes, M. W., 2000: Techniques for forecasting the cessation of lightning at Cape Canaveral Air Station and the Kennedy Space Center, M. S. Thesis, Air Force Institute of Technology, 90 pp.
- Istok, M. J., and co-authors, 2009: WSR-88D dual polarization initial operational capabilities. *25<sup>th</sup> Conference on International Interactive Information and Processing Systems (IIPS) for Meteorology, Oceanography, and Hydrology*, Amer. Meteor. Soc., Phoenix, AZ, Paper 15.5.
- Jayarathne, E.R., Saunters, C.P.R. and Hallett, J., 1983. Laboratory studies of the charging of soft-hail during ice crystal interactions. *Q. J. R. Meteorol. Soc.*, 109: 609-630.
- Krehbiel, P. R., Brooke, M. and McCrory, R. A., 1979: An analysis of the charge structure of lightning discharges to ground *J. Geophys. Res.*, **84**, 2432-2456.
- \_\_\_\_\_, 1986: The electrical structure of thunderstorms, in *The Earth's Electrical Environment*, National Academy Press, Washington, D.C., pp. 90 - 113.
- Koshak, W.J., and Coauthors, 2004: North Alabama Lightning Mapping Array (LMA): VHF source retrieval algorithm and error analysis. *J. Atmos. Oceanic Technol.*, **21**, 543-558.
- Lakshmanan, V., K. Hondl, and R. Rabin, 2009: An efficient, general-purpose technique for identifying storm cells in geospatial images. *J. Ocean. and Atmos. Tech.*, **26** (3), 523-537.
- \_\_\_\_\_, T. Smith, G. J. Stumpf, and K. Hondl, 2007: The warning decision support system – integrated information (WDSS-II). *Wea. Forecasting*, **22** (3), 592-608.
- \_\_\_\_\_, T. Smith, 2009: Data mining storm attributes from spatial grids. *J. Atmos. Oceanic Technol.*, **26**, 2353-2365.
- McNamara, T. M., 2002: The horizontal extent of cloud-to-ground lightning over the Kennedy Space Center. M.S. Thesis, Air Force Institute of Technology, 114 pp.
- \_\_\_\_\_, 2009: Four dimensional lightning surveillance system's (4DLSS) application in space launch weather support. Southern Thunder Workshop, Cocoa Beach, FL, July 27-30.
- Melvin, H. A., H.E. Fuelberg, 2010: Characteristics of decaying storms during lightning cessation at Kennedy Space Center and Cape Canaveral Air Force Station, *3<sup>rd</sup> Intl. Lightning Meteor. Conf.*, 21-22 April, 1-17.
- \_\_\_\_\_, J. E. Glover, 2005: Preliminary results from phase-1 of the statistical forecasting of lightning cessation project. Conf. on Meteor. App. of Lightning Data, 9-13 January, 6 pp.
- Ryzhkov, A. and Giangrande, S. (2004) Measurements of rain with polarimetric WSR-88D radar. Operational demonstration. In: Sixth International Symposium on Hydrological Applications of Weather Radar. Melbourne, Australia.
- Rudlosky, S. D., 2010: Pre- and Post-upgrade Distributions of NLDN Reported Cloud-to-Ground Lightning Characteristics in the Contiguous United States. *Monthly Weather Review*. *138*(9), 3623-3633. DOI:10.1175/2010MWR3283.1.



- Saunders, C.P.R., Keith, W.D. and Mitzeva, R.P., 1991. The effect of liquid water on thunderstorm charging. *J. Geophys. Res.*, 96:11,007-11,017.
- Scharfenberg, K., 2006: A functional description of the NSSL polarimetric hydrometeor classification algorithm. Report of the National Severe Storms Laboratory, 9 pp.
- Shao, X.M. and P.R. Krehbiel, The spatial and temporal development of intracloud lightning, submitted to *J. Geophys. Res.* (1995).
- Stano, G. T., H. E. Fuelberg, and W. P. Roeder, 2010: Developing an empirical lightning cessation forecast guidance for the Kennedy Space Center, *J. Geophys. Res.*, 115, D09205, doi:10.1029/2009JD13034.
- Takahashi, T., 1973: Electrification of growing ice crystals. *J. Atmos. Sci.*, **30**, 1220-1224.
- Williams, E. R. 2001: The electrification of severe storms. *Severe Convective Storms, Meteor. Monogr.*, No. 50, Amer. Meteor. Soc., 527-561.
- Wolf, P., 2006: Anticipating the initiation, cessation, and frequency of cloud-to-ground lightning, utilizing WSR-88D reflectivity data. NOAA/National Weather Service, Jacksonville, Florida.
- Woodard, C. J., L. D. Carey, W. A. Petersen, and W. P. Roeder, 2012: Operational Utility of Dual-Polarimetric Variables in Lightning Initiation Forecasting. *Electronic J. Operational Meteor.* Early Review.